

Spike-Timing Dependence of Structural Plasticity Explains Cooperative Synapse Formation in the Neocortex

Moritz Deger^{1*}, Moritz Helias², Stefan Rotter^{1,3}, Markus Diesmann^{1,2,4}

1 Bernstein Center Freiburg, Albert-Ludwig University, Freiburg, Germany, **2** Computational and Systems Neuroscience, Institute of Neuroscience and Medicine (INM-6), Research Center Jülich, Jülich, Germany, **3** Faculty of Biology, Albert-Ludwig University, Freiburg, Germany, **4** Medical Faculty, RWTH Aachen University, Aachen, Germany

Abstract

Structural plasticity governs the long-term development of synaptic connections in the neocortex. While the underlying processes at the synapses are not fully understood, there is strong evidence that a process of random, independent formation and pruning of excitatory synapses can be ruled out. Instead, there must be some cooperation between the synaptic contacts connecting a single pre- and postsynaptic neuron pair. So far, the mechanism of cooperation is not known. Here we demonstrate that local correlation detection at the postsynaptic dendritic spine suffices to explain the synaptic cooperation effect, without assuming any hypothetical direct interaction pathway between the synaptic contacts. Candidate biomolecular mechanisms for dendritic correlation detection have been identified previously, as well as for structural plasticity based thereon. By analyzing and fitting of a simple model, we show that spike-timing correlation dependent structural plasticity, without additional mechanisms of cross-synapse interaction, can reproduce the experimentally observed distributions of numbers of synaptic contacts between pairs of neurons in the neocortex. Furthermore, the model yields a first explanation for the existence of both transient and persistent dendritic spines and allows to make predictions for future experiments.

Citation: Deger M, Helias M, Rotter S, Diesmann M (2012) Spike-Timing Dependence of Structural Plasticity Explains Cooperative Synapse Formation in the Neocortex. *PLoS Comput Biol* 8(9): e1002689. doi:10.1371/journal.pcbi.1002689

Editor: Olaf Sporns, Indiana University, United States of America

Received: May 10, 2012; **Accepted:** July 26, 2012; **Published:** September 20, 2012

Copyright: © 2012 Deger et al. This is an open-access article distributed under the terms of the Creative Commons Attribution License, which permits unrestricted use, distribution, and reproduction in any medium, provided the original author and source are credited.

Funding: This work was partially funded by BMBF Grant 01GQ0420 to the BCCN Freiburg, the Helmholtz Alliance on Systems Biology, the Next-Generation Supercomputer Project of MEXT, and EU Grant 269921 (BrainScaleS). The funders had no role in study design, data collection and analysis, decision to publish, or preparation of the manuscript.

Competing Interests: The authors have declared that no competing interests exist.

* E-mail: deger@bcf.uni-freiburg.de

Introduction

The structure of neocortical networks of neurons changes in time: new synapses are formed, mature, and eventually are pruned again, in the adult as well as in the developing animal [1,2], for recent reviews see [3,4,5]. The majority (about 90%) of excitatory synaptic contacts terminate on dendritic spines [6], and dendritic spines almost always (96%) form a synapse [7]. The synapses on dendritic spines are highly dynamic [8,9], for example [10] found an average spine turnover of 5.7%/day in primary visual cortex and of 15.4%/day in somatosensory cortex. Yet in the adult animal, the statistics of the numbers of synapses are preserved over time, indicating that synapse creation and pruning balance each other [11,12,13]. According to theoretical studies on associative networks, structural plasticity enhances the memory capacity of a network substantially [14,15], and has been shown to be related to motor learning in the brain [16].

The three studies [17,18,19] reported the distributions of numbers of synaptic contacts for different intra-cortical synapses in rat somatosensory cortex. Fares et al. [20] subsequently analyzed whether the reported distributions could result from random and independent synaptic contact formation, given a set of potential sites (close appositions) between axons and dendrites of reconstructed cells. As they showed, independent formation of synaptic contacts alone cannot explain the distributions. In addition a

cooperative pruning mechanism, by which synaptic contacts that constitute a single synapse stabilize each other, is required to explain the observed distributions.

Here we build on grounds of this work and go beyond it in two aspects: Primarily, we consider synaptic processes that operate continuously in time. Secondly, we investigate an explicit candidate mechanism for the cooperation between synaptic contacts: Local correlation detection at the dendritic spines and thus dependent pruning and maturation of spines.

Recently Kasai et al. [21] summarized known properties of the plasticity of dendritic spines. Their model [22] describes the dynamics of the volume of dendritic spines. Here we restrict this model to three distinct categories of synapse states and introduce an explicit spike-timing dependence. Other models of structural plasticity [23,24,25] are based on the firing rate of the neurons. Consequently, in these models spike-timing and correlations of the spiking activity do not play a role, so they cannot show the mechanism of synaptic cooperation that we hypothesize here. The relative timing of pre- and postsynaptic activity indeed influences structural plasticity at the dendritic spine [26]. In contrast to previous models, the model of Helias et al. [27] is sensitive to the spike-timing of the pre- and the postsynaptic cell and describes structural plasticity in biophysical terms of protein kinetics in response to synaptic input. Here we choose an intermediate scale by still describing single synaptic contacts, but with a higher level

Author Summary

Structural plasticity has been observed even in the adult mammalian neocortex – in seemingly static neuronal circuits structural remodeling is continuously at work. Still, it has been shown that the connection patterns between pairs of neurons are not random. In contrast, there is evidence that the synaptic contacts between a pair of neurons cooperate: several experimental studies report either zero or about 3–6 synapses between neuron pairs. The mechanism by which the synapses cooperate, however, has not yet been identified. Here we propose a model for structural plasticity that relies on local processes at the dendritic spine. We combine and extend the previous models and determine the equilibrium probability distribution of synaptic contact numbers of the model. By optimizing the parameters numerically for each of three reference datasets, we obtain equilibrium contact number distributions that fit the references very well. We conclude that the local dendritic mechanisms that we assume suffice to explain the cooperative synapse formation in the neocortex.

of abstraction than previous work [22,27]. The goal of the present work is to demonstrate the potential of local correlation detection at the spine, while making minimal assumptions about the involved biophysical processes. The assumptions entering our model, as introduced in detail in Methods, required to qualitatively explain the experimental results, are: a) presynaptic release of glutamate causes postsynaptic depolarization at excitatory synapses, b) depolarization electrically spreads within the dendrite, c) there is a correlation sensing mechanism sensitive to the relative time of presynaptic and postsynaptic firing (e.g. NMDA receptors) that causes downstream effects on the evoked synaptic amplitude in a spike timing dependent plasticity (STDP, [28]) like manner, d) synapses with small amplitude are more likely to be pruned than strong ones. Because of its analytical tractability, we can compute the steady state of our model and match its parameters to experimental reference data, analogous to Fares et al. [20]. Our results show that no direct signaling between synaptic contacts is necessary to explain cooperative synapse formation. In contrast, it suffices that distinct synaptic contacts cooperate in exciting the postsynaptic neuron, and thereby indirectly affect spike-timing dependent structural plasticity at other synaptic contacts.

Methods

In this section we introduce a model of structural plasticity and describe the optimization procedure to fit the model to the experimental reference data.

Correlation trace at the synaptic contact

Let us first introduce a simple model for the correlation detection at the postsynaptic dendritic spine. An action potential of the postsynaptic neuron causes a depolarization at the site of each dendritic spine. The spine has the biophysical substrate to maintain a signal that depends on the time of the action potential in relation to the time when a presynaptic impulse arrived [27]. Here, we call this signal the correlation trace $q(t)$ and assume a phenomenological model: if the presynaptic neuron spiked shortly before the postsynaptic one, the correlation trace is increased by 1. We call this a causal event. For the opposite relative timing, called an anti-causal event, the trace is decreased by 1. The trace therefore counts causal and anti-causal combinations of pre- and

postsynaptic spikes. Further we assume that the correlation trace is forgetful: it has a leak with the time constant $\tau > 0$, and we also assume that there is some additive noise in the process. The dynamics of the correlation trace at the synapse is given by the stochastic differential equation [29]

$$\frac{d}{dt}q(t) = -\frac{1}{\tau}q(t) + g(t)s(t) + \eta(t), \quad (1)$$

where $s(t) = \sum_k \delta(t - t_k)$ is the spike train of the postsynaptic neuron, with the spike times $\{t_k\}$, the factor $g(t) \in \{-1, 1\}$ specifies if the particular spike is counted as a causal or anti-causal event, and $\eta(t)$ is an additional white noise with mean zero $\langle \eta \rangle = 0$ and infinitesimal variance ξ^2 . Mathematically, the trace $q(t)$ is identical to a shot noise [30] with the exponential kernel $h(t) = \theta(t)e^{-t/\tau}$ driven by the stochastic input process $g(t)s(t) + \eta(t)$.

Let us now introduce a minimal model of correlated spiking of the neurons. For each postsynaptic spike, we speak of a causal event at a given synaptic contact if the closest spike of the presynaptic neuron occurred prior to the postsynaptic one (because it could have caused the postsynaptic spike). If the closest presynaptic spike occurred after the postsynaptic one, the event is called anti-causal. Suppose that the probability for a causal event is given by p . If both of the neurons fire independently, then $p = 0.5$. We define $g(t) = 1$ with probability p and $g(t) = -1$ with probability $1 - p$ for each postsynaptic spike in $s(t)$.

Strictly speaking, the process defined by (1) is unphysical, since through $g(t)$ it depends on events in the near future (because the time of the next presynaptic spike has to be known). We hence consider (1) as an effective, adiabatic description of the correlation trace, since we are only interested in the statistics of the trace on long timescales. A process like (1) could result from several biophysical implementations that do in fact respect causality. For example the synaptic weights in phenomenological models of spike timing dependent plasticity, for which causal implementation are known [31] follow dynamics similar to (1). An example of a cellular mechanism to implement (1) is the number of activated CaMKII macro-molecules [27] or long-term potentiation [32,33,34].

Now let us further assume that postsynaptic spikes $s(t)$ occur according to a Poisson point process with rate v . The firing rate v comes about through integration of thousands of synaptic inputs, and the particular synaptic connection modeled here only provides a small contribution to v . Since structural plasticity is known to be a slow process compared to the activity of neurons, and since the time constant of possible candidate mechanisms for the correlation trace can be considerable [35], a large integration time constant τ is reasonable, such that $v\tau \gg 1$. Then the equilibrium probability distribution of q is a normal distribution with mean μ and variance σ^2 ,

$$\mu = \tau v(p - (1 - p)) = \tau v(2p - 1) \quad (2)$$

$$\sigma^2 = \frac{1}{2} \tau (v(p + (1 - p)) + \xi^2) = \frac{1}{2} \tau (v + \xi^2). \quad (3)$$

Eqs. (2, 3) can be obtained by considering two independent stochastic processes $q_s(t)$ and $q_\eta(t)$ with $\dot{q}_s = -\tau^{-1}q_s + s$ and $\dot{q}_\eta = -\tau^{-1}q_\eta + \eta$. Then $q = q_s + q_\eta$ and mean and variance of q follow from summing the respective statistics of q_s and q_η , which can be obtained using standard techniques [30]. Note that σ^2 is independent of p .

The probability of causal spike pairings p depends on the number of active synapses x connecting the presynaptic neuron to the postsynaptic one, because each excitatory synapse increases the chance of the presynaptic neuron to make the postsynaptic neuron fire. As demonstrated for integrate-and-fire neurons in [36], the probability of a spiking response to a presynaptic spike is proportional to the synaptic weight of the input spike for a wide range of magnitudes of the synaptic strength. If the membrane potential of the postsynaptic neuron integrates the inputs linearly, the synaptic weight of the input from the presynaptic neuron is proportional to the number of active synaptic contacts between the neurons. So the probability of a spike response, and so of a causal event, rises proportionally to the number of active synaptic contacts. Effectively we thus assume $p(x) = p_0 + x\Delta$, where x is the number of active synaptic contacts between the presynaptic to the postsynaptic neuron, Δ is the response probability per synapse, and $p_0 = 0.5$. The two components of the probability $p(x)$ can be interpreted as the probability p_0 for a causal event by chance due to the Poisson firing of the postsynaptic neuron with rate v and the probability $x\Delta$ exceeding chance level triggered by the arrival of the presynaptic spike.

In order to obtain an estimate of Δ consider a single synaptic contact between two neurons that, upon activation, causes an excitatory postsynaptic potential (EPSP) with amplitude w . For a leaky integrate-and-fire model neuron in the asynchronous state [37] resembling cortical activity, we can read off the response probability P_r of a neuron to such a voltage jump from Fig. 4D in [36]. So we have $\Delta = P_r(w) \approx wm$ with $m = 0.05(\text{mV})^{-1}$. The respective values of the EPSP size w per contact have been reported along with the reference datasets in [17,18,19], and we list them among the model parameters in Tab. 1. We thus arrive at the estimate for the probability of a correlated pairing

$$p(x) = p_0 + mw x, \quad (4)$$

and thus with (2) the mean of the stationary distribution of $q(t)$ is

$$\mu(x) = \tau v(2p_0 - 1 + 2mw x). \quad (5)$$

Note that the linear model (4) for the probability of causal spike pairings may for large x and w yield values of $p(x) > 1$, which are nonsensical. A consistent definition of $p(x)$ should saturate when reaching the value 1. Taking into account this saturation at large x , however, would not make a difference for the models considered here, because all solutions for synapse distributions found below exhibit vanishing probability throughout at such large values of x .

So far, we hypothesized a generic correlation detection mechanism at each synaptic contact and computed its equilibrium statistics (5) and (3) for multiple excitatory contacts between two neurons. In our model the values of the correlation trace of each synaptic contact follow a normal distribution, specified by its mean $\mu(x)$ and variance σ^2 , which depend on the parameters τ, v, ξ . Note that only the mean $\mu(x)$ depends on the number x of active contacts, whereas σ^2 is a constant. To reduce the amount of free parameters of the model, we further set $v = 5\text{Hz}$ which is a reasonable choice for neocortical neurons.

Structural plasticity based on the synaptic correlation trace

The synaptic correlation trace can guide structural plasticity. Because of a lack of detailed knowledge about the biomolecular mechanisms involved [38] we again employ a simple effective model. As structural plasticity is a slow process compared to the

spiking activity of neurons, we assume that the distribution of the correlation trace at each synaptic contact is effectively in stochastic equilibrium throughout. This is also known as an adiabatic approximation. Let us now assume that a structural change of the synaptic contact is initiated when the correlation trace crosses a boundary value θ . A biochemical mechanism underlying this assumption could be the activation of a signaling pathway when a specific number of activated CaMKII molecules is reached [39]. Given the random trajectory of the correlation trace q , we need to know how long it takes until q crosses the boundary upon which the synaptic contact makes the transition. This is known as a first passage time problem with an absorbing boundary. The inverse of the mean first passage time is called the escape rate. For simplicity, let us approximate q as a Brownian motion with the same infinitesimal mean and variance as the actual process (1). Then, according to the Arrhenius approximation [40], the escape rate is

$$\propto e^{-(\theta - \mu(x))^2 / \sigma^2} \quad (6)$$

in the case that the values of q are far from the boundary θ , such that $|\theta - \mu| \gg \sigma$. Here the proportionality constant is called the Arrhenius constant. Now what happens to the rate of structural changes when μ approaches θ ? If we take the model of a boundary crossing process seriously, then the escape rate should diverge as $\mu \rightarrow \theta$. However, in a biological system it is more plausible that the rate of structural changes converges to a certain maximum rate which the cellular machinery can achieve. Based on this argument we construct our model for the rate of structural changes by extrapolating from the Arrhenius approximation (6), forcing it to eventually converge to a plateau,

$$\kappa(\alpha, \theta, \mu, \sigma) = \begin{cases} |\alpha| e^{-(\theta - \mu(x))^2 / \sigma^2} & \text{if } \alpha(\theta - \mu(x)) > 0 \\ |\alpha| & \text{else} \end{cases}, \quad (7)$$

with $\alpha \in \mathbb{R}$. Depending on the sign of α , $\kappa(x)$ either approaches or departs from the plateau for increasing $\mu(x)$.

As our assumptions about the biophysical implementation are quite general, they can model maturation, shrinkage and pruning of a synaptic contact alike. However, these are distinct processes that take place during different stages in the life cycle of a synaptic contact. For example, we cannot assume that the correlation detector noise ξ has the same magnitude for small and large dendritic spines since the number of channels mediating the signal might be different for the two. Therefore we use the model (7) for maturation, shrinkage and pruning, but choose a different set of transition parameters $\{\alpha, \theta\}$ and correlation trace noise ξ for each case. We decorate quantities associated to maturation with m , those associated to shrinkage with s and pruning with p . So the rate of maturation transitions is defined as

$$\lambda_m(x) = \kappa(\alpha_m, \theta_m, \mu(x), \sigma_m), \quad (8)$$

the rate of shrinkage transitions as

$$\lambda_s(x) = \kappa(\alpha_s, \theta_s, \mu(x), \sigma_s), \quad (9)$$

and the rate of pruning as

$$\lambda_p(x) = \kappa(\alpha_p, \theta_p, \mu(x), \sigma_p). \quad (10)$$

The correlation trace parameters $\{\tau, v, \Delta, p_0\}$ are assumed to be identical for both thin spines (inactive synaptic contacts) and large

Table 1. Reference data, optimized parameter sets and properties of the structural plasticity models.

Connection	L4-L2/3	L5-L5	L4-L4		
Reference	[17]	[18]	[19]		
w [mV]	0.0813	0.63	0.44		
$\langle N \rangle$ [1]	4.040 ± 5.010	5.998 ± 7.312	4.368 ± 5.358		
displayed in	Fig. 1a	Fig. 1b	Fig. 2a	Fig. 1c	Fig. 2b
τ [s]	$1.28E+09$	$3.95E+08$	$2.74E+05$	$4.32E+11$	$2.74E+05$
ξ_m [$1/\sqrt{s}$]	511.109	$3.80E+03$	31.955	$1.75E+05$	31.955
ξ_s [$1/\sqrt{s}$]	449.392	1.844	30.974	0.330	30.974
α_m [λ_c]	$-4.33E+06$	$-3.68E+04$	$-3.90E+04$	$-1.85E+06$	$-3.90E+04$
α_s [λ_c]	$-6.80E+10$	$-2.63E+08$	$-7.82E+09$	$-4.99E+04$	$-7.82E+09$
θ_m [1]	$1.82E+08$	$3.90E+08$	$6.53E+04$	$5.55E+10$	$6.53E+04$
θ_s [1]	64.259	$2.07E+06$	$-1.61E+04$	$1.04E+11$	$-1.61E+04$
λ_i [λ_c]	346.847	18.029	3.129	4.345	3.129
R [1]	0.0008	0.0460	0.4926	0.0447	0.1808
$\langle x \rangle$ [1]	0.091 ± 0.633	0.182 ± 0.931	0.151 ± 0.729	0.545 ± 1.265	0.489 ± 1.076
$\langle y \rangle$ [1]	$4.66E-04 \pm 0.022$	0.020 ± 0.174	0.114 ± 0.619	0.045 ± 0.297	0.252 ± 0.755
$\langle x+y \rangle$ [1]	0.091 ± 0.637	0.202 ± 1.041	0.265 ± 1.269	0.590 ± 1.421	0.740 ± 1.680
Corr[x,y] [1]	0.148	0.581	0.772	0.440	0.674
$d\langle x \rangle/dp_0$ [1]	398.016	12.782	-22.455	-34.488	153.283
$d\langle y \rangle/dp_0$ [1]	1.789	1.495	-16.185	-2.474	62.665
$d\langle x+y \rangle/dp_0$ [1]	399.804	14.277	-38.641	-36.962	215.948
$\langle T_s \rangle$ [$1/\lambda_c$]	$2.60E-04$	0.009	0.032	0.013	0.130
$\langle T_a \rangle$ [$1/\lambda_c$]	0.407	0.896	3.165	0.384	471.925
λ_c [1/day]	$3.56E-04$	$5.38E-04$	$7.11E-04$	$2.41E-03$	$3.14E-03$
$\langle T_s \rangle$ [days]	0.731	16.151	45.242	5.204	41.450
$\langle T_a \rangle$ [days]	1144.198	1667.021	4453.517	159.640	150234.202

Description of listed values top to bottom: Section 1) Connection properties: Unitary EPSP amplitude w per contact as published in the reference, expected number of close appositions N from [20] and standard deviation of N , figure in which properties of the model with this parameter set are displayed; Section 2) Model parameters: Correlation trace time constant τ (1), amplitude ξ of correlation trace noise, scale α of transition rates (see eq. 7 and Fig. 1c), saturation threshold θ , intrinsic maturation/shrinkage/pruning rate λ_i ; Section 3) Model properties: Sum of squared residuals R of the model (see eq. 19), expected numbers of active (x), inactive (y) and total ($x+y$) synaptic contacts and standard deviation of $x, y, x+y$, Pearson correlation coefficient of x and y , derivatives of expectation of x, y and $x+y$ with respect to the probability of causal spike pairings (p_0) (estimated numerically), expected lifetimes of inactive and active contacts (see eq. 23 and eq. 24), estimate of model time scale λ_c to match physiological spine turnover ratio (25), lifetimes in units of days using λ_c estimate. Additional, fixed parameters that are common to all models are $m=0.05(\text{mV})^{-1}$, $p_0=0.5$ and $v=5\text{Hz}$.

doi:10.1371/journal.pcbi.1002689.t001

spines (active synaptic contacts), which will be defined below. The pruning rate uses the same parameters as shrinkage, except for the noise magnitude ξ of maturation, because pruning is assumed to take place in thin spines.

Apart from the activity dependent transitions, the model also includes intrinsic fluctuations as in [22], see Fig. 1B. We assume that random maturation (enlargement), shrinkage and pruning of a spine occurs constantly with the rate λ_i , and the creation of new thin spines with rate λ_c .

Let us summarize the structural plasticity model we have introduced. At each of the synaptic contacts between a pair of neurons, a correlation trace is formed by counting causal and anti-causal pre-post spike pairings. The distribution of the values of the correlation trace depends on the number of active synaptic contacts since they all contribute to firing the postsynaptic neuron. We have further assumed that the activity-dependent structural changes of synaptic contacts depend on the correlation traces. Finally we also included intrinsic fluctuations of the synapse configuration.

Steady state of the synapse

Above we defined a model for structural plasticity for the synapse between a pre- and a postsynaptic neuron. Although in this model the individual synaptic contacts may continuously change, the state of the synapse develops towards a stable steady state. A synapse typically consists of many individual synaptic contacts, as depicted in Fig. 1A. The neocortex is densely packed with only very limited unoccupied extracellular space. Accordingly, pairs of neurons cannot form arbitrary numbers of synaptic contacts [41]. Fares et al. [20] investigated reconstructed cortical tissue and counted the numbers of close appositions between pairs of neurons. At such a close apposition a synaptic contact may form, but is not necessarily present. Describing these results statistically, a probability distribution for the number of close appositions N between two neurons can be obtained [20].

At each of the close appositions, the neurons may form a synaptic contact; in our model, we treat the different volumes of spines and EPSP amplitudes in a coarse-grained fashion, distinguishing just three different states for each contact to occupy

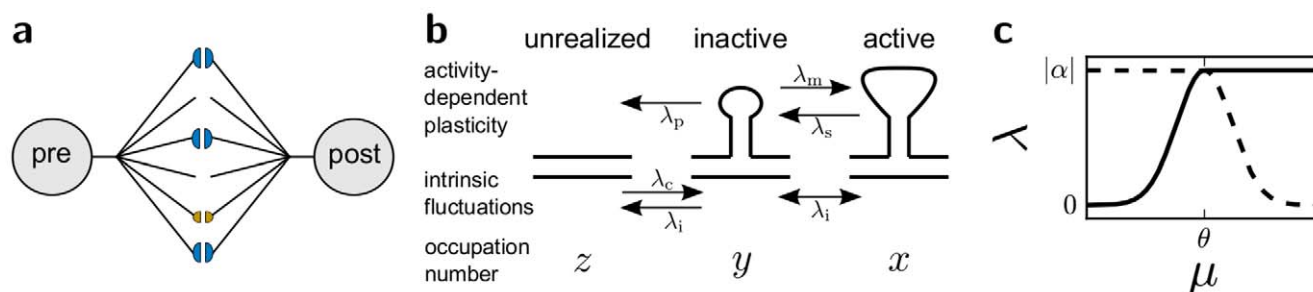


Figure 1. Illustrations. **a**: Schematic of a synapse connecting a pair of cortical neurons (pre- and postsynaptic). Individual synaptic contacts can be active (blue, larger; corresponding to a large dendritic spine), inactive (orange, smaller; corresponding to a thin dendritic spine) or unrealized. **b**: State diagram of the structural plasticity model adapted from [22]. A synaptic contact can occupy one of three states: active, inactive or unrealized. Transitions from one state to the other are possible through either intrinsic fluctuations or activity-dependent plasticity, indicated by the arrows. The transitions from unrealized to inactive are called “creation” (rate λ_c), from inactive to active “maturation” (rates λ_m and λ_i). The transitions from active to inactive are called “shrinkage” (rates λ_s and λ_i) and from inactive to unrealized “pruning” (rates λ_p and λ_i). A synapse consists of N close appositions which may or may not host inactive or active synaptic contacts. The occupation number of the three states, active, inactive, unrealized are called x , y and z , respectively. **c**: Assumed functional form of the dependence of the rate of activity dependent transitions (λ_m , λ_s , λ_p) on the mean value μ of the correlation trace, which is formed at the dendritic spine. The absolute value of α sets the scale of the transition rate, while its sign flips the function from right-saturating (solid) to left-saturating (dashed). The parameter θ determines at what correlation level saturation of the transition rate is reached.

doi:10.1371/journal.pcbi.1002689.g001

– active, inactive, or unrealized. An active synaptic contact here describes a larger dendritic spine that contains both AMPA and NMDA receptors. An inactive contact models a thin, either newly formed or recently shrunk dendritic spine that has much less AMPA receptors [42,43] and contributes little to firing the postsynaptic neuron. An unrealized contact, finally, is a close apposition where no contact has formed, but might be formed in the future. It is a close apposition without an established synaptic contact and corresponds to the potential synapse in [20]. A similar model has previously been proposed in the context of associative networks [44,45].

We denote the numbers of synaptic contacts in these three states by x , y and z respectively. Since at any time $x + y + z = N$, the state of a synapse is unambiguously defined by the combination of the number of active and inactive contacts (x, y). Now consider an ensemble of independent synapses, each with the maximum contact number N . The probability $p_{x,y}$ of a synapse to be in the state (x, y) evolves in time according to the Master equation [46]

$$\begin{aligned} \frac{d}{dt} p_{(x,y)} = & -p_{(x,y)}[(x+2y)\lambda_i + (N-x-y)\lambda_c \\ & + x\lambda_s(x) + y\lambda_p(x) + y\lambda_m(x)] \\ & + (x+1)p_{(x+1,y-1)}[\lambda_s(x+1) + \lambda_i] \\ & + (y+1)p_{(x,y+1)}[\lambda_p(x) + \lambda_i] \\ & + (y+1)p_{(x-1,y+1)}[\lambda_m(x-1) + \lambda_i] \\ & + (N-x-y+1)p_{(x,y-1)}\lambda_c. \end{aligned} \quad (11)$$

The first term sums up the rate of leaving the state (x, y) by all possible transitions. The second and third terms sum up all possibilities to go into state (x, y) from other states by shrinkage and pruning, and the fourth term by maturation. The last term considers the transitions due to the creation of inactive synapses, the rate of which is given by λ_c (see also Fig. 1B). The steady state distribution does not depend on the time scale of the transition rates, so we can consider the constants $\alpha_m, \alpha_s, \alpha_i$ in units of λ_c . The time scale of the structural plasticity is then set by $1/\lambda_c$. In (25) below we will see how the value of λ_c can be determined by experimental data.

To determine the steady state configuration of the synapse, let us introduce a numbering of all the possible synaptic states $\{(x, y) | x + y \leq N\}$, such that the probability of each state $p_{(x,y)}$ is represented by the value p_i , with a one to one correspondence between indices i and states (x, y). Then (11) can be written as

$$\frac{d}{dt} \vec{p} = M \vec{p} \quad (12)$$

where the entries of the matrix M can be read off the Master equation. Since M describes a Markov process it is column-stochastic (which means all columns sum up to zero). Since the process is irreducible, according to the Perron-Frobenius theorem there is only one stationary solution. We can determine the stationary probability distribution $\vec{p}^0(N)$ by solving $M \vec{p}^0 = 0$ under the constraint that $\sum_i p_i^0 = 1$. We implemented the construction of the matrix M efficiently using Cython [47] and solved for the stationary solution using Scientific Python [48].

The stationary distribution depends on the number of close appositions N . [20] have estimated the distribution $P(N)$ for the three types of intra-cortical connections that we consider. We incorporate this by determining $\vec{p}^0(N)$ for each N separately, and subsequently compute the averaged distribution

$$p_i^{\text{avg}} = \sum_{N=0}^{N_{\text{max}}} P(N) p_i^0(N). \quad (13)$$

Fares et al. [20] provide the distribution $P(N)$ for N up to $N_{\text{max}} = 20$.

For comparison with the reference datasets (see below), we are merely interested in the marginal probability of a certain total number n of synaptic contacts, disregarding whether they are active or inactive. The marginalization can be obtained from \vec{p}^{avg} by summing over all states (x', y') with $x' + y' = n$, or more conveniently phrased as

$$P(n) = \sum_i p_i^{\text{avg}} 1_{x(i)+y(i)=n}, \quad (14)$$

where the function $x(i)$ returns the value of x of the state (x, y) with index i , and 1_Q equals 1 if Q is true and 0 otherwise. Analogously, the marginal average distributions of the number of active and inactive synapses are

$$P(x) = \sum_i P_i^{\text{avg}} 1_{x(i)=x}, \quad (15)$$

$$P(y) = \sum_i P_i^{\text{avg}} 1_{y(i)=y}. \quad (16)$$

Comparison to reference data and model optimization

In the experimental studies [17,18,19] a set of occurrence frequencies f_n of numbers of synaptic contacts $n \geq 1$ for several pairs of neurons was obtained, each for three different types of intra-cortical projections. Complementing this, for the same three datasets, the probability P_{con} of a pair of neurons to be connected with at least one active contact can be estimated [20]. The distribution of the numbers of active synaptic contacts serve as reference data in our study. For each of the three datasets, we transform the reported data to the probability mass function

$$P_{\text{ref}}(n) = \begin{cases} 1 - P_{\text{con}} & n = 0 \\ \frac{f_n}{\sum_n f_n} P_{\text{con}} & n \geq 1 \end{cases}. \quad (17)$$

we evaluate (14) and obtain the residuals

$$r_n = \frac{P(n) - P_{\text{ref}}(n)}{\max_{n \geq 1} \{P_{\text{ref}}(n)\}}, \quad (18)$$

for $n \geq 1$. The residuals are scaled by the maximum of the reference distribution to enable comparison of the quality of the fits across reference datasets. We minimize the sum of squared residuals

$$R = \sum_{x=1}^{N_{\text{max}}} r_x^2 \quad (19)$$

using the Levenberg-Marquardt algorithm, applying its implementation from Scientific Python [48]. We call R the error of the model. The optimization problem has several local minima, so we initialize the optimization procedure at many points in the 8-dimensional parameter space and compare the values of R to which the optimization converged. Specifically, we choose four different initial values in each parameter dimension, which makes a total of $4^8 = 65536$ distinct optimization runs per reference dataset. The parameter sets which resulted in a minimal value of R are shown in Tab. 1, along with additional information on the model, and the resulting equilibrium distributions are shown in Fig. 2.

We also obtained parameter sets which yield good fits to two reference distributions simultaneously. The resulting distributions for the connections L4-L4 and L5-L5 are displayed in Fig. 3. Here the fit error was defined as the sum of the errors (19) of both distributions, $R = R_{\text{L4-L4}} + R_{\text{L5-L5}}$. With respect to this the same optimization procedure was performed.

Lifetime of synapses and turnover ratio

Here we compute the average lifetime of an inactive synaptic contact and of an active contact in the equilibrium state of the

synapse model, see Fig. 1a for the possible transitions. We define the lifetime T as the expected time until the contact is pruned. Consider an active contact in a synapse. It may become an inactive contact either through intrinsic or activity dependent shrinkage. The mean time up to the transition from active to inactive is $t_{\text{ia}}(x) = 1/(\lambda_i + \lambda_s(x))$. An inactive contact, on the other hand, might make a transition to the active state (maturation), which would take the time $t_{\text{ai}}(x) = 1/(\lambda_i + \lambda_m(x))$, or to the unrealized state (pruning) in the time $t_{\text{pi}} = 1/(\lambda_i + \lambda_p(x))$. The mean time until the first transition, either maturation or pruning, is $\hat{t}_i(x) = 1/(t_{\text{ai}}^{-1}(x) + t_{\text{pi}}^{-1})$. Either of the two transitions happens with a probability given by the fraction of rates involved, $P_{\text{ai}}(x) = t_{\text{ai}}^{-1}(x)\hat{t}_i(x)$ and analogously $P_{\text{pi}}(x) = t_{\text{pi}}^{-1}(x)\hat{t}_i(x) = 1 - P_{\text{ai}}(x)$. If the inactive contact becomes active, then it will become inactive eventually, and subsequently might be pruned or become active again. Accounting for the possible paths the inactive contact may take upon its first transition we obtain the expected lifetime of the inactive contact as

$$T_i(x) = P_{\text{pi}}(x)\hat{t}_i(x) + P_{\text{ai}}(x)(\hat{t}_i(x) + T_a(x+1)), \quad (20)$$

where $T_a(x)$ is the lifetime of an active contact in a synapse that has x active contacts. In turn, starting from an active contact just adds one active to inactive transition, so

$$T_a(x) = t_{\text{ia}}(x) + T_i(x-1). \quad (21)$$

Inserting (21) and the definitions above into (20) yields

$$T_i(x) = \frac{\hat{t}_i(x) + t_{\text{ia}}(x+1)P_{\text{ai}}(x)}{1 - P_{\text{ai}}(x)}. \quad (22)$$

We average the lifetimes across the equilibrium probability distribution of synapse states and obtain

$$\langle T_i \rangle = \sum_N P(N) \sum_i p_i^0(N) T_i(x(i)) \quad (23)$$

$$\langle T_a \rangle = \sum_N P(N) \sum_i p_i^0(N) T_a(x(i)). \quad (24)$$

To match the time scale of structural development of our model to what is known from in-vivo studies we compute the spine turnover ratio as it is defined in [10],

$$\text{TOR} = \frac{n_{\text{gained}} + n_{\text{lost}}}{2n_{\text{total}}}. \quad (25)$$

Here n_{gained} and n_{lost} are the numbers of gained and lost spines during a given period of time, and n is the number of spines observed. In our model, the expectation values of these quantities are given as

$$n_{\text{gained}} = \sum_N P(N) \sum_i p_i^0(N) \lambda_c z(i)$$

$$n_{\text{lost}} = \sum_N P(N) \sum_i p_i^0(N) (\lambda_p(x(i)) + \lambda_i) y(i)$$

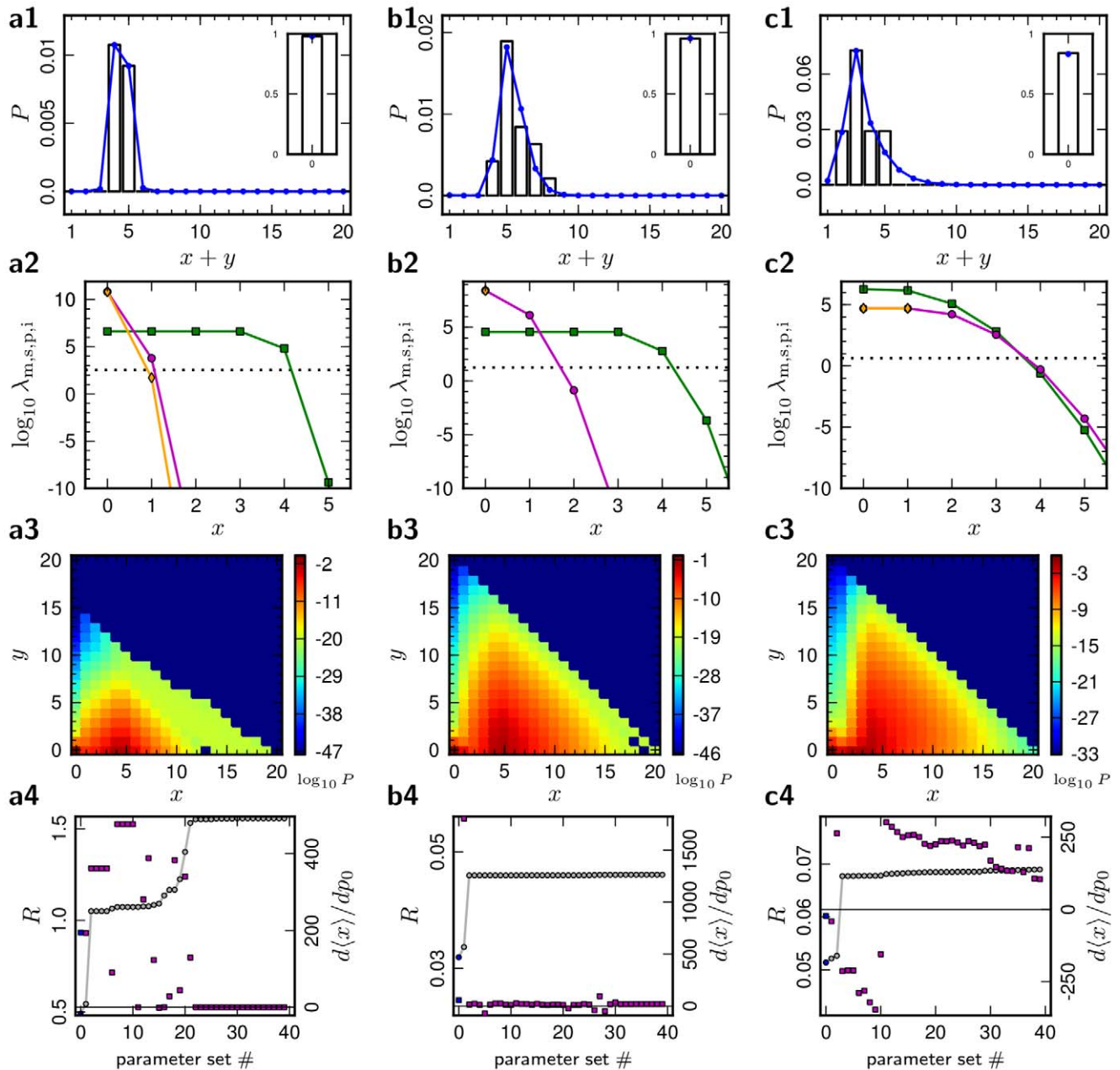


Figure 2. Single synaptic connection models. Best-fit individual models of the synaptic connections L4–L23 (**a**), L5–L5 (**b**) and L4–L4 (**c**). **a1,b1,c1** (row 1): Equilibrium distributions of the total number of synaptic contacts in the structural plasticity model (blue, eq. 14) compared to reference data (black). **a2,b2,c2** (row 2): Transition rate functions (7) of the models in the row 1, respectively, in units of λ_c . Activity dependent maturation rate $\lambda_m(x)$ (green squares, eq. 8), shrinkage rate $\lambda_s(x)$ (orange diamonds, eq. 9), pruning rate $\lambda_p(x)$ (magenta circles, eq. 10) and intrinsic maturation, shrinkage, and pruning rate λ_i (dotted line). The spine creation rate λ_c sets the time scale and has a value of $\log_{10} \lambda_c = 0$. **c1,c2,c3** (row 3): Joint equilibrium distribution of the number of active (x) and inactive (y) synapses. **a4,b4,c4** (row 4): Fit error (R , gray) and derivatives of active synaptic contact number with respect to baseline correlation ($d\langle x \rangle / dp_0$, magenta) for the best 40 parameter sets, ordered by error R . Blue markers indicate the model that is displayed above (rows 1 to 3). Model parameters and further information are given in Table 1. doi:10.1371/journal.pcbi.1002689.g002

$$n_{\text{total}} = \sum_N P(N) \sum_i p_i^0(N) (x(i) + y(i)),$$

where λ_p and λ_i are given in units of λ_c . So we obtain TOR_{λ_c} in units of λ_c from (25). In rat somatosensory cortex [10] found $\text{TOR} = 15.4\%/ \text{day}$. Accordingly (25) sets the time scale λ_c of the model to $\lambda_c = 15.4\%/ \text{day} / \text{TOR}_{\lambda_c}$.

Necessity of inactive synapses for explanation of experimentally observed distributions of synaptic contacts

In this section we consider a simplified version of our model which does not include inactive synaptic contacts (thin spines). In that model, at a close apposition there can be either no synaptic contact or an active synaptic contact. Between these two states transitions are allowed just as between the inactive and the active

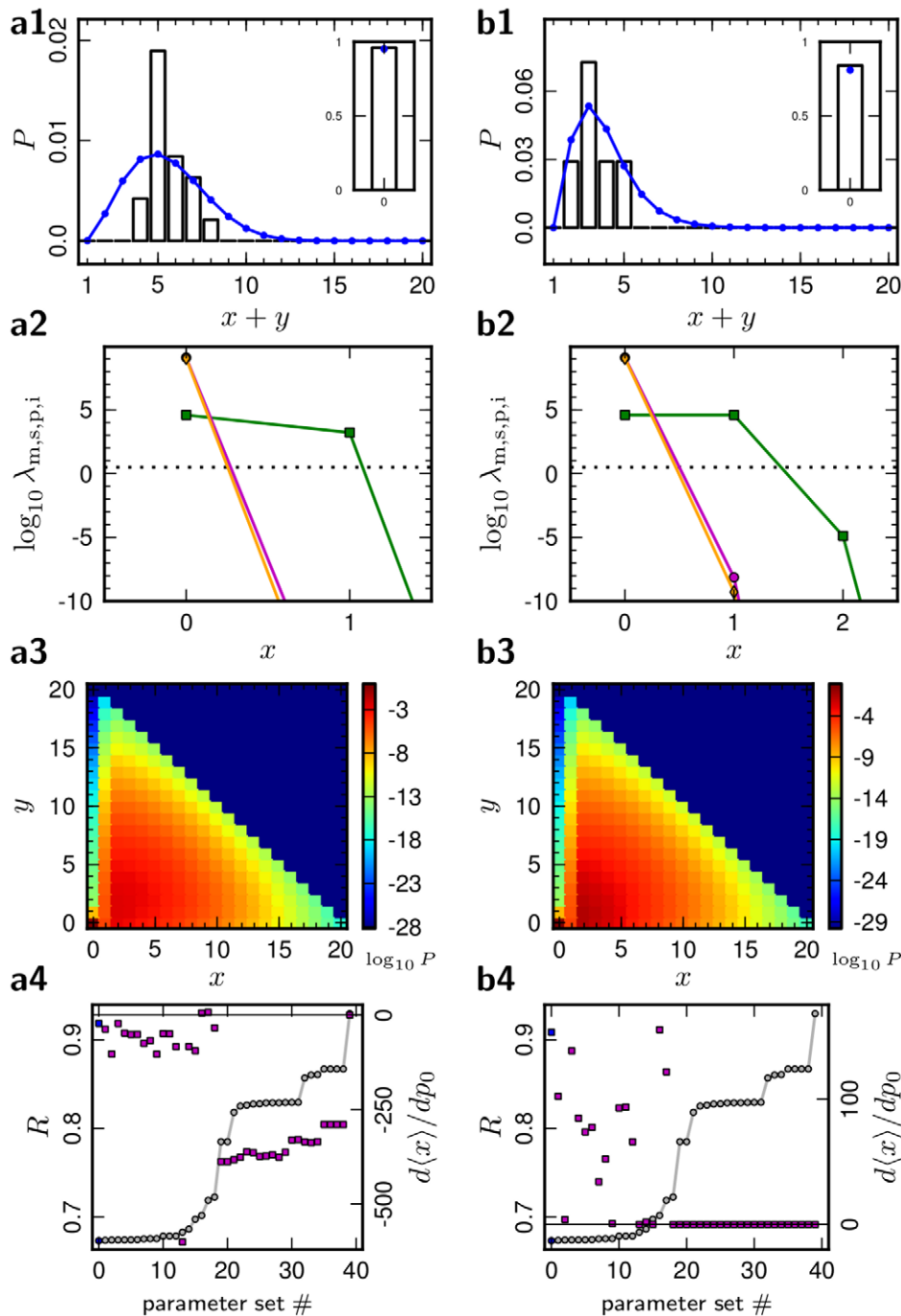


Figure 3. Model of two synaptic connections. Best-fit model for both synaptic connections L5-L5 (a) and L4-L4 (b) (same model parameters). **a1,b1-a4,b4** (rows 1 to 4) as in Fig. 2. Model parameters and further information are given in Table 1. doi:10.1371/journal.pcbi.1002689.g003

state in the full model (see Fig. 1B), but here we call them $\lambda_c(x)$ (creation) and $\lambda_p(x)$ (pruning), which may yet be arbitrary functions. Assume there are N close apposition between a pair of neurons. Then the state of the synapse is defined by the number of active connections x . Let us denote the probability of the state x by p_x here. In stochastic equilibrium the probability fluxes into and out of the state x must balance, so for $0 \leq x \leq N-1$ it must hold that

$$0 = (N-x)\lambda_c(x)p_x - (x+1)\lambda_p(x+1)p_{x+1}$$

from which follows that

$$\frac{p_{x+1}}{p_x} = \frac{N-x}{x+1} \frac{\lambda_c(x)}{\lambda_p(x+1)}. \quad (26)$$

Now consider the case of $x=0$. In all three reference datasets, $P_{\text{ref}}(1)/P_{\text{ref}}(0)=0$, as can be seen in Fig. 2a1–a3. According to (26) this requires $\lambda_c(0)/\lambda_p(1)=0$, which can only be achieved by $\lambda_c(0)\rightarrow 0$ or $\lambda_p(1)\rightarrow \infty$. In contrast, around the secondary peak of the reference distributions P_{ref} , (26) entails that λ_c and λ_p must be of comparable magnitude. More specifically, the right hand side of expression (26) has to change from values larger than 1 to values smaller than 1 as x passes the secondary peak from below. To satisfy these requirements, even only approximately, demands highly non-monotonous choices of the functions $\lambda_c(x)$ and $\lambda_p(x)$ that are difficult to justify biophysically. Once the model includes the intermediate state of the inactive synaptic contact, however, it is possible to find biologically plausible parameter sets to explain the reference distributions, as described in the rest of the paper.

Results

Overview of the model

Kasai et al. [22] monitored the temporal evolution of the volume of dendritic spines and described it as a random walk with volume dependent drift and diffusion components. According to their findings, newly formed dendritic spines are small, and accumulate AMPA receptors as the spine volume increases. Thus a small spine can grow or disappear, and a large spine can shrink. Spines of all volumes, however, were found to contain NMDA receptors [42]. The study by Holtmaat et al. [10] suggests that thin spines are more readily pruned than thick spines, and that they may be of a lower efficacy or NMDA receptor-only (inactive) synapses. It was previously suggested [43,49] that small spines might correspond to silent synaptic contacts. In our model, we distinguish between only three states that each synaptic contact can occupy: active, inactive and unrealized, without considering the spine volume and channel density of the dendritic spines explicitly. These states correspond, respectively, to large spines, thin spines and close appositions with no spine, as illustrated in Fig. 1b. Note that we do not claim that the functional distinction between thin and large spines is actually as clear-cut as assumed in the model – the model merely represents a coarse-grained spine state. In this model, transitions between the three morphological/functional states are possible. Following [22] and [50], such transitions can occur either due to intrinsic fluctuations, or depending on the activity of the pre- and postsynaptic neuron. Note also that, although the inactive synaptic contact is allowed as a transitional state, it turns out to rarely occur in the optimized models that will be discussed below.

The basic idea of the model put forward in this study is the following: As described in [27] dendritic spines have the biomolecular capability of detecting correlations in the relative spike timing of the pre- and postsynaptic neuron. If there are several active excitatory synaptic contacts from a presynaptic neuron to a single postsynaptic cell, all these synaptic contacts contribute to elicit spikes in the postsynaptic neuron. Hence each of the contacts increases the correlation between the two cells, measurable at each of the corresponding dendritic spines. So even if there is no direct communication between the synaptic contacts, they affect each other indirectly by increasing the correlation of pre- and postsynaptic spikes. Spike-timing dependence of structural plasticity is thus a candidate mechanism for the cooperation between synaptic contacts.

According to [27] the magnitude of calcium influx into the dendritic spine depends on the proximity of pre- and postsynaptic spikes in time. The calcium influx activates or deactivates CaMKII macro-molecules and thus leaves a local memory. We call such a memory of the spike-timing correlation a correlation trace. The

activation of the CaMKII subunits can be preserved for a long time [51]. The model we consider here, however, does not rely on the biophysical details of CaMKII activation, but just assumes a correlation trace is available. For the purpose of this study, the correlation trace could also come about by other mechanisms.

Employing this correlation trace, we introduce a phenomenological model for activity dependent maturation, shrinkage and pruning of spines depending on the correlation of the spike-timing of pre- and postsynaptic cell, as described in detail in Methods. The model is based on [22] and incorporates the basic properties of structural plasticity [21], activity-independent creation and pruning of spines, intrinsic fluctuations of spine volume, and activity-dependent spine remodeling. The set of all synaptic contacts connecting a given pair of neurons constitute a synapse, see also Fig. 1a. The state of a synapse is defined by the number of active contacts (large spines) x and inactive contacts (thin spines) y . The time-evolution of the synapse state is then described as a Markov process. For a given parameter set, we solve for the stationary probability distribution of the states (x,y) .

Fits to reference data

The parameters of the model were then optimized so that the distribution of the total number of synaptic contacts reproduces the experimental reference data, shown in Fig. 2a1–c1, along with the respective transition rates of the model (6) in a2–c2. For each of the three reference datasets (a, b, c), we show the best model that resulted from the optimization. The models can reproduce the experimental distributions of synapse numbers.

The existence of such a stationary distribution means that the average numbers of inactive, active and potential sites of the synapse do not change in time. This is so despite the constant creation and pruning of synaptic contacts since these processes compensate each other in equilibrium. Implicitly, the model allows that inactive, active and potential sites coexist between a given pair of neurons.

The parameter sets for the displayed models are given in the second section of Tab. 1. The fit of the connection L4–L23 takes very different parameter values than the others. Nonetheless for all three modeled connections, the time constant τ of the correlation trace is large compared to the time scale of fluctuations of neuronal activity, in agreement with our assumption about the distribution of the correlation trace. Concerning the parameters of the activity dependent structural plasticity, we find qualitatively similar results across datasets: In all three cases, both maturation and shrinkage/pruning rates decrease with increasing active synapse number, granting long-term stability to established synapses.

The models of the intralaminar connections L4–L4 and L5–L5 show remarkable similarities. Both have a comparable τ and the rate of intrinsic, activity independent transitions λ_i is low, although this was not an a priori assumption. The parameter values for α and θ are difficult to interpret individually. Across all the models, inactive synaptic contacts are rare, as indicated by the fraction of $\langle y \rangle / \langle x \rangle$ which ranges between 0 and 0.5. A fit of both connections L4–L4 and L5–L5 with a single parameter set is displayed in Fig. 3. Although the model distributions in Fig. 3a1,b1 do not follow the reference data as closely as in Fig. 2, a good agreement of the distributions and the reference is achieved.

Properties of the optimized models

For each of the three reference datasets we obtained many models with a comparable fit error R . Fig. 2a4–c4 and Fig. 3a4,b4 show the error R (circles) of the best parameter sets obtained, ordered by the value of R . We also investigate how the model

distribution changes in response to an increase in the baseline probability of causal spike pairing. Some models decrease their contact number, while other models increase it, as can be seen from the derivative $d\langle x \rangle / dp_0$ (squares in Fig. 3, 1, row 4). This quantity can take very different values for comparable fit errors R . We call a model Hebbian if the number of active contacts grows upon an increase of causal spike pairings ($d\langle x \rangle / dp_0 > 0$). Conversely we call a model anti-Hebbian if the number of contacts decreases ($d\langle x \rangle / dp_0 < 0$). This diversity indicates that the plasticity model used here is general enough to implement Hebbian and anti-Hebbian learning, depending on the parameters. In Tab. 1 the value of the derivative $d\langle x \rangle / dp_0$ is given along with other properties of the selected models. For each dataset, we selected the best model irrespective of it being Hebbian or anti-Hebbian. Another characteristic property of a model is the joint distribution of active synapses x and inactive synapses y (Fig. 2 and 2, row 3). Especially in the model connections L4-L4 and L5-L5 x and y tend to be strongly correlated. While the expectation value of $x + y$ is largely determined by the reference data, the smaller expectation value of y indicates that only a small proportion of spines are small and functionally weak. The marginal distribution of active and inactive synapses are shown for the three best models in Fig. 4a. In all selected models, across the datasets, the expectation values of x and y do not sum up to the expectation value of the number of contacts N , which means that many unrealized synapses (close appositions without inactive or active contacts) are present, consistent with experimental findings [21].

Fig. 4b addresses the question whether a homeostasis of the neuronal firing rate can be achieved by this structural plasticity model. Here, a homeostasis means that an increase in firing rate leads to pruning of input synapses, thus lowering the firing rate in effect. Conversely a decrease in firing rate should lead to synapse maturation. If that is the case, the plasticity rule establishes a homeostatic control of the firing rate to a fixed value. In our model, a negative derivative $d\langle x \rangle / dv$ means that the plasticity rule acts as a firing rate homeostasis. From Eq. (5) we conclude that a change in v can either increase or decrease the value of $\mu(x)$ for a given x , depending on the value of the baseline correlation p_0 . Previously, we arbitrarily set p_0 to 0.5. However, given a parameter set, we can change the value of p_0 to p'_0 without changing the transition rates (and all equilibrium properties of the model) if we also shift the thresholds to

$$\theta' = 2\tau v(p'_0 - p_0) + \theta, \quad (27)$$

because then all the distances $\mu(x) - \theta$ to the threshold are preserved. Thus p_0 is effectively a free parameter of the model and can be adjusted to set $d\langle x \rangle / dv$, as is shown in Fig. 4b. Hence the structural plasticity model we propose can establish a firing rate homeostasis.

Furthermore we derived the expected lifetime of a synapse in the model, which is also shown in Tab. 1. Here the lifetime is defined as the expected time until the synapse is pruned. Before being pruned, it can go back and forth between the states inactive and active several times (fluctuate in volume). The lifetime is very different for inactive and for active synapses, the latter exceeding the former by about one order of magnitude or more. This is due to the fact that typically several active contacts coexist and mutually stabilize, which entails small rates λ_m , λ_s and λ_p (cf. Fig. 2 row 2). If an active synapse becomes inactive, the rate to go back to the active state also increases, which promotes going back and forth through these states. This behavior matches nicely with the volume fluctuations of large dendritic spines described in [22].

Through (25) finally we can relate the time scale λ_c of the models to experimental data [10]. The values for λ_c are listed in Tab. 1 and confirm our assumption of a time scale separation of structural plasticity and neuronal activity. Using this estimate of the timescale, the lifetimes of inactive contacts are about a couple of days, while the lifetimes of active contacts span from a month up to years. [10] called spines with a lifetime of less than 8 days transient, and spines with longer lifetimes persistent. This distinction roughly applies to the lifetimes of inactive and active contacts in our model.

Discussion

We propose a model of structural plasticity to explain cooperative synapse formation [20]. The transitions of the states of synapses are assumed to depend on a signal locally available to a spine that depends on the correlation between pre- and postsynaptic activity, the correlation trace. There is strong evidence that a correlation trace could indeed be implemented in the dendritic spine through phosphorylation of the macromolecule CaMKII [35,27,34]. CaMKII has also been shown to be necessary for structural and long-term plasticity [52,53,4], and may also drive presynaptic changes [54]. Here we assume an abstract, effective correlation trace instead of explicitly modeling the dynamics of CaMKII. This makes our results independent of the specific mechanisms employed at the synaptic contact, since also other processes may be available to form the correlation trace. We assume the correlation trace at the spine is forgetful, such that it integrates causal and anti-causal spike pairing events like a leaky integrator with a certain time constant. This time constant affects the location of the equilibrium probability distribution of the correlation trace and its variance. Across the datasets L4-L4 and L5-L5, the time constants are comparable. If the correlation trace is implemented biologically by the cycle of expression, activation and degradation of CaMKII, these time constants will be observable in experiments. The optimized values for the time constant τ are well in the range of possible values that sustained CaMKII activation can show [51] for all three reference datasets. The differences in the model parameters of the connection L4–L23 compared to the other two intralaminar connections might be explained by the finding that most synaptic contacts of this connection are formed on dendritic shafts rather than on spines [55]. At dendritic shafts functionally similar plasticity mechanisms could be at work, but our model might be less appropriate for this type of connection. However, although in early postnatal development more shaft synapses exist, in later stages synapses on spines dominate [56,57].

The rates of structural changes at the synapse are assumed to be a function of the equilibrium correlation trace distribution. To model this dependence mathematically we chose a versatile functional form (7). This is necessary since a comprehensive quantitative description of the correlation dependence of structural plasticity is not known to date. Our optimization results for the transition rates show a strong selectivity for specific numbers of active contacts in a synapse: Transition rates are much higher in case there are few active contacts between two neurons, and many active contacts stabilize the system in all of the three modeled intra-cortical synapse types. Future experiments could investigate whether synaptic contact number (or EPSP amplitude) correlates with calcium transient amplitudes at the spines and with rates of spine maturation, shrinkage and pruning.

Using the optimized models we also computed the expected lifetimes synaptic contacts. The lifetime of active contacts is about ten to one hundred times larger than the lifetime of inactive

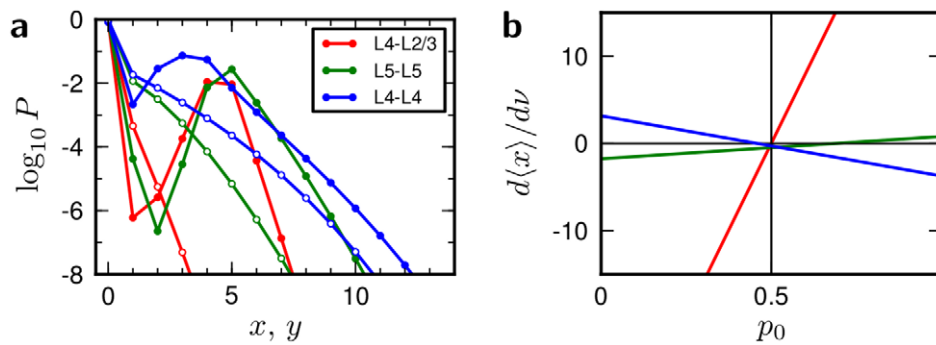


Figure 4. Further properties of the single connection models. *a*. Marginal probabilities of active (x , filled circles, eq. 15) and inactive (y , empty circles, eq. 16) synaptic contact numbers of the best-fit models shown in Fig. 1. *b*. Derivative of the number of active synaptic contacts by the neuronal firing rate as a function of the baseline correlation p_0 – values of the θ_m and θ_s are shifted to keep the equilibrium distribution unchanged for all values of p_0 (27). Negative values indicate a stable equilibrium (firing rate homeostasis). Colors as in *a*. doi:10.1371/journal.pcbi.1002689.g004

contacts across our models. This can be understood given the experimental references' results that an active contact is always accompanied by several others. For such synapses, our models predict a vanishing rate of activity dependent transitions, which lets the synapses stay in the active state for a long time. Thus persistent spines here correspond to active contacts, and transient spines to inactive contacts. Our finding constitutes a statistical explanation of the existence of these two distinct classes of spines [10].

Our best-fit models show functional differences. Most notably, the models can be either Hebbian or anti-Hebbian, in the sense that an increase in the frequency of causal spike pairing leads to either increased or decreased numbers of active contacts. Both Hebbian and anti-Hebbian connections have been observed in the neocortex [58]. For all connections we found comparably good fits of both types. Furthermore our model predicts a joint probability distribution of active and inactive contacts which goes beyond current experimental references. Future experiments which determine both of these numbers for many neuron pairs will allow further evaluation of our model. A possibility to optically distinguish and monitor active and inactive synapses in experiments might be to use fluorescent markers for AMPA and NMDA receptors. Synaptic contacts that what we call “inactive” should show less AMPA than “active” ones, but the inactive ones also include those synapses with few AMPA receptors.

Previous models of structural plasticity have assumed a homeostasis of the firing rate [59,3], in the sense that if neuronal activity increases beyond an a-priori chosen set-point, synaptic contacts are pruned to decrease the excitatory drive, and the reverse for activity below the set-point. Indeed the correlation dependent structural plasticity model [27] shows this behavior. We have investigated whether our models show firing rate homeostasis by computing how the expected number of active contacts changes with the firing rate. This dependency can be chosen arbitrarily by adjusting a free parameter of the model (see Fig. 4b). Our model hence is capable of providing the proposed firing-rate homeostasis for properly chosen parameters.

To obtain a simple Markov process, we used the discrete categories “unrealized”, “inactive” and “active” to describe the state of a synaptic contact. Technically our model is similar to the cascade synapse model of [60] but adds the morphological interpretation of the synaptic states. The inactive contact might be closely related to silent synapses, but in the actual biological system such a clear-cut distinction between functional states can probably not be made, see for example [38]. Busetto et al. [61] found that

silent synapses are abundant in the developing animal but vanish in the adult. However, only spines that were morphologically mature were included in their study, making no claim about existence of thin spines with small heads. Quantal EPSC analysis in the adult neocortex showed that close to all synaptic contacts of the connection L4–L23 are functional [55]. Our model of this connection also shows no inactive synapses in expectation, which renders them unobservable in practice. Further [62] find in cultured hippocampal slices that newly formed spines contain AMPA receptors. Small spines, however, are generally easy to miss, since they are often smaller than the resolution limit of optical microscopy [10,61], and they may also be pruned again quickly after formation [63]. After all there is ample evidence that newly formed spines are small [21] and that AMPA receptor density correlates with volume [22]. We thus follow [43] and approximate thin, small spines as inactive synaptic contacts, and large spines as active ones as described above in detail.

As a consequence of the coarse-grained description of the state of synaptic contacts, all active synaptic contacts in our model produce an EPSP of a fixed amplitude w . However, in biology this amplitude varies from contact to contact. Including a fine grained description of synaptic amplitudes in a structurally similar model as the one presented here would result in a massive increase of the dimension of the state space and is therefore potentially unfeasible. Such a dispersion of synaptic amplitudes would result in a different functional dependence of the mean (2) and variance (3) of the correlation trace q on the number of active contacts x . However, at a given synapse the mean would still be monotonically increasing with x . On a population level, the dispersion of synaptic amplitudes thus results in an additional contribution to the width of the distribution of the correlation trace q in (3). We can think of part of the noise $\eta(t)$ added to q as representing this contribution. This reduces the precision of correlation detection at the dendritic spine. In a model with dispersion of synaptic amplitudes, we therefore expect to find qualitatively similar fits for our coarse grained model at a correspondingly reduced additional noise.

We defined that inactive synaptic contacts host NMDA receptors. The conductance of NMDA receptors increases upon a postsynaptic depolarization if the magnesium block is removed. At negative voltages NMDA channels have a smaller but non-vanishing conductance and hence mediate excitatory postsynaptic currents (EPSC). However, the time scale of NMDA activation is much slower than that of AMPA channels. A postsynaptic action potential partially caused by NMDA currents of one synaptic

contact would thus occur much later than the presynaptic glutamate release. The postsynaptic depolarization is therefore less efficient in opening the NMDA receptors at another synaptic contact of the same synapse. This, however, is the crucial mechanism that allows correlation detection and cooperation in our model. Hence one may assume that NMDA currents contribute much less to the correlation trace, and thus have vanishing impact on the cooperative plasticity of our model. We therefore use the term “inactive” here in a functional sense.

In neonatal rat hippocampus also presynaptically silent synapses have been observed, which show a very low probability of transmitter release [64,65]. However, even a low probability of release enables the formation of a postsynaptic correlation trace at the dendritic spine as in our model. Moreover, even presynaptic changes of the transmitter release have been reported to depend on such a correlation trace in a similar way [54]. The dependence of maturation and shrinkage/pruning on the correlation trace that we use here is a sufficiently generic model to also include these presynaptic mechanisms, although we do not intend to model them here explicitly.

The term structural plasticity describes a broad range of phenomena, many of which have not been addressed here. Competition between synapses from distinct neurons to a common postsynaptic neuron has been shown to be important for the emergence of cortical network structure [66]. In the more detailed models of structural plasticity in neuronal networks based on the activity of CaMKII [27,67], cooperation and competition between synaptic contacts necessarily occurs. Here we assumed that

synapses between different pairs of neurons develop independently, so inter-synaptic competition effects were not considered. Furthermore, structural plasticity also includes changes to the network structure that can come about by migration of axons on much longer time scales. Our model rather describes the steady state of the adult cortex, during which spines form and retract, but the axonal arborization can be assumed to be constant [13]. In lesion studies it has been shown that the steady state can become unstable and axons again begin to migrate [68].

Although simple and abstract in its description of complex cellular phenomena, our model can explain the cooperation of synaptic contacts in the adult neocortex, postulated in [20]. The model shows how continuously active structural plasticity can lead to the global configuration of synaptic contact numbers that was observed experimentally. The key ingredient of the model which mediates the necessary cooperation is a trace of the spike-timing correlations of the pre- and postsynaptic neuron. The resulting synaptic learning rule is local (it solely requires mechanisms at the synaptic contacts) but can nonetheless explain cooperative synapse formation.

Author Contributions

Conceived and designed the experiments: M. Deger, M. Helias, S. Rotter, M. Diesmann. Performed the experiments: M. Deger, M. Helias, S. Rotter, M. Diesmann. Analyzed the data: M. Deger, M. Helias, S. Rotter, M. Diesmann. Contributed reagents/materials/analysis tools: M. Deger, M. Helias. Wrote the paper: M. Deger, M. Helias, S. Rotter, M. Diesmann.

References

- Globus A, Scheibel AB (1966) Loss of dendrite spines as an index of pre-synaptic terminal patterns. *Nature* 212: 463–465.
- Raisman G (1969) Neuronal plasticity in the septal nuclei of the adult rat. *Brain Res* 14: 25–48.
- Butz M, Wörgötter F, van Ooyen A (2009) Activity-dependent structural plasticity. *Brain Res Rev* 60: 287–305.
- Kasai H, Fukuda M, Watanabe S, Hayashi-Takagi A, Noguchi J (2010) Structural dynamics of dendritic spines in memory and cognition. *Trends Neurosci* 33: 121–129.
- Fu M, Zuo Y (2011) Experience-dependent structural plasticity in the cortex. *Trends Neurosci* 34: 177–187.
- Harris KM, Kater SB (1994) Dendritic spines: cellular specializations imparting both stability and excitability to synaptic function. *Annu Rev Neurosci* 17: 341–371.
- Arellano JI, Espinosa A, Fairén A, Yuste R, DeFelipe J (2007) Non-synaptic dendritic spines in neocortex. *Neuroscience* 145: 464–469.
- Bonhoeffer T, Yuste R (2002) Spine motility: phenomenology, mechanisms, and function. *Neuron* 35: 1019–1027.
- Trachtenberg JT, Chen BE, Knott GW, Feng G, Sanes JR, et al. (2002) Long-term in vivo imaging of experience-dependent synaptic plasticity in adult cortex. *Nature* 420: 788–794.
- Holtmaat AJ, Trachtenberg JT, Wilbrecht L, Shepherd GM, Zhang X, et al. (2005) Transient and persistent dendritic spines in the neocortex in vivo. *Neuron* 45: 279–291.
- Stepanyants A, Hof PR, Chklovskii DB (2002) Geometry and structural plasticity of synapse connectivity. *Neuron* 34: 275–288.
- Stepanyants A, Hirsch J, Martinez LM, Kisvarday ZF, Ferecsko AS, et al. (2008) Local potential connectivity in cat primary visual cortex. *Cereb Cortex* 18: 13–28.
- Escobar G, Fares T, Stepanyants A (2008) Structural plasticity of circuits in cortical neuropil. *J Neurosci* 28: 8477–8488.
- Chklovskii DB, Mel BW, Svoboda K (2004) Cortical rewiring and information storage. *Nature* 431: 782–788.
- Knoblauch A, Palm G, Sommer FT (2010) Memory capacities for synaptic and structural plasticity. *Neural Comput* 22: 289–341.
- Xu T, Yu X, Perlik AJ, Tobin WF, Zweig JA, et al. (2009) Rapid formation and selective stabilization of synapses for enduring motor memories. *Nature* 462: 915–919.
- Feldmeyer D, Lübke J, Silver RA, Sakmann B (2002) Synaptic connections between layer 4 spiny neuron/layer 2/3 pyramidal cell pairs in juvenile rat barrel cortex: physiology and anatomy of interlaminar signalling within a cortical column. *J Physiol (Lond)* 538: 803–822.
- Markram H, Lübke J, Frotscher M, Roth A, Sakmann B (1997) Physiology and anatomy of synaptic connections between thick tufted pyramidal neurons in the developing rat neocortex. *J Physiol (Lond)* 500: 409–440.
- Feldmeyer D, Egger V, Lübke J, Sakmann B (1999) Reliable synaptic connections between pairs of excitatory layer 4 neurones within a single ‘barrel’ of developing rat somatosensory cortex. *J Physiol (Lond)* 521: 169–190.
- Fares T, Stepanyants A (2009) Cooperative synapse formation in the neocortex. *Proc Natl Acad Sci U S A* 106: 16463–16468.
- Kasai H, Hayama T, Ishikawa M, Watanabe S, Yagishita S, et al. (2010) Learning rules and persistence of dendritic spines. *Eur J Neurosci* 32: 241–249.
- Yasumatsu N, Matsuzaki M, Miyazaki T, Noguchi J, Kasai H (2008) Principles of long-term dynamics of dendritic spines. *J Neurosci* 28: 13592–13608.
- Damasch JE, Wagner GP, Wolff JR (1986) Self-stabilization of neuronal networks. i. the compensation algorithm for synaptogenesis. *Biol Cybern* 54: 211–222.
- Butz M, Teuchert-Noodt G (2006) A simulation model for compensatory plasticity in the prefrontal cortex inducing a cortico-cortical dysconnection in early brain development. *J Neural Transm* 113: 695–710.
- van Ooyen A, van Pelt J, Corner MA (1995) Implications of activity dependent neurite outgrowth for neuronal morphology and network development. *J Theor Biol* 172: 63–82.
- Tanaka Ji, Horiike Y, Matsuzaki M, Miyazaki T, Ellis-Davies GCR, et al. (2008) Protein synthesis and neurotrophin-dependent structural plasticity of single dendritic spines. *Science* 319: 1683–1687.
- Helias M, Rotter S, Gewaltig M, Diesmann M (2008) Structural plasticity controlled by calcium based correlation detection. *Front Comput Neurosci* 2: 7.
- Morrison A, Diesmann M, Gerstner W (2008) Phenomenological models of synaptic plasticity based on spike timing. *Biol Cybern* 98: 459–478.
- Gardiner CW (1983) *Handbook of Stochastic Methods for Physics, Chemistry and the Natural Sciences*. Number 13 in Springer Series in Synergetics. Berlin: Springer-Verlag.
- Papoulis A (1991) *Probability, Random Variables, and Stochastic Processes*. 3rd edition. New York: McGraw-Hill, Inc.
- Morrison A, Diesmann M, Gerstner W (2008) Phenomenological models of synaptic plasticity based on spiketiming. *Biol Cybern* 98: 459–478.
- Markram H, Lübke J, Frotscher M, Sakmann B (1997) Regulation of synaptic efficacy by coincidence of postsynaptic APs and EPSPs. *Science* 275: 213–215.
- O’Donnell C, Nolan MF, van Rossum MCW (2011) Dendritic spine dynamics regulate the long-term stability of synaptic plasticity. *J Neurosci* 31: 16142–16156.
- Lisman J, Yasuda R, Raghavachari S (2012) Mechanisms of calcium action in long-term potentiation. *Nat Rev Neurosci* 13: 169–182.
- Lisman J, Schulman H, Cline H (2002) The molecular basis of CaMKII function in synaptic and behavioral memory. *Nat Rev Neurosci* 2: 175–190.
- Helias M, Deger M, Rotter S, Diesmann M (2010) Instantaneous non-linear processing by pulse-coupled threshold units. *PLoS Comput Biol* 6: e1000929.

37. Brunel N (2000) Dynamics of sparsely connected networks of excitatory and inhibitory spiking neurons. *J Comput Neurosci* 8: 183–208.
38. McMahon SA, Diaz E (2011) Mechanisms of excitatory synapse maturation by trans-synaptic organizing complexes. *Curr Opin Neurobiol* 21: 221–227.
39. Lisman J (1989) A mechanism for Hebb and anti-Hebb processes underlying learning and memory. *Proc Natl Acad Sci U S A* 86: 9574–9578.
40. Chandrasekhar S (1943) Stochastic problems in physics and astronomy. *Rev Mod Phys* 15: 1–89.
41. Stepanyants A, Chklovskii DB (2005) Neurogeometry and potential synaptic connectivity. *Trends Neurosci* 28: 387–394.
42. Matsuzaki M, Ellis-Davies GCR, Nemoto T, Miyashita Y, Iino M, et al. (2001) Dendritic spine geometry is critical for ampa receptor expression in hippocampal cal pyramidal neurons. *Nat Neurosci* 4: 1086–1092.
43. Matsuzaki M, Honkura N, Ellis-Davies GCR, Kasai H (2004) Structural basis of long-term potentiation in single dendritic spines. *Nature* 429: 761–766.
44. Knoblauch A (2006) On compressing the memory structures of binary neuronal associative networks. Technical Report HRI-EU 06-02, Honda Research Institute Europe GmbH, D-63073 Offenbach/Main, Germany.
45. Knoblauch A (2009) The role of structural plasticity and synaptic consolidation for memory and amnesia in a model of cortico-hippocampal interplay. In: Mayor J, Ruh N, Plunkett K, editors. *Connectionist Models of Behavior and Cognition II: Proceedings of the 11th Neural Computation and Psychology Workshop*. Singapore: World Scientific, pp. 79–90.
46. van Kampen NG (1992) *Stochastic Processes in Physics and Chemistry*. Amsterdam: North-Holland: Elsevier Science Publishers.
47. Behnel S, Bradshaw R, Seljebotn DS, Ewing G, et al. (2009). Cython: C-Extensions for Python, version 0.11.2-1. Available: <http://www.cython.org>.
48. Jones E, Oliphant T, Peterson P, et al. (2001–). SciPy: Open source scientific tools for Python, version 0.7.0-2. Available: <http://www.scipy.org>.
49. Atwood HL, Wojtowicz MJ (1999) Silent synapses in neural plasticity: Current evidence. *Learn Mem* 6: 542–571.
50. Minerbi A, Kahana R, Goldfeld L, Kaufman M, Marom S, et al. (2009) Long-term relationships between synaptic tenacity, synaptic remodeling, and network activity. *PLoS Biol* 7: 1000136.
51. Miller P, Zhabotinsky AM, Lisman JE, Wang XJ (2005) The stability of a stochastic camkii switch: Dependence on the number of enzyme molecules and protein turnover. *PLoS Biol* 3: e107.
52. Shouval HZ, Bear MF, Cooper LN (2002) A unified model of NMDA receptor dependent bidirectional synaptic plasticity. *Proc Natl Acad Sci U S A* 99: 10831–10836.
53. Shouval H, Castellani G, Blais B, Yeung L, Cooper L (2002) Converging evidence for a simplified biophysical model of synaptic plasticity. *Biol Cybern* 87: 383–391.
54. Pratt KG, Watt AJ, Griffith LC, Nelson SB, Turrigiano GG (2003) Activity-dependent remodeling of presynaptic inputs by postsynaptic expression of activated camkii. *Neuron* 39: 269–281.
55. Silver RA, Lubke J, Sakmann B, Feldmeyer D (2003) High-probability unquantal transmission at excitatory synapses in barrel cortex. *Science* 302: 1981–1984.
56. Braitenberg V, Schüz A (1991) *Anatomy of the Cortex: Statistics and Geometry*. Berlin, Heidelberg, New York: Springer-Verlag.
57. Yuste R, Bonhoeffer T (2004) Genesis of dendritic spines: insights from ultrastructural and imaging studies. *Nat Rev Neurosci* 5: 24–34.
58. Tzounopoulos T, Rubio ME, Keen JE, Trussell LO (2007) Coactivation of pre- and postsynaptic signaling mechanisms determines cell-specific spike-timing-dependent plasticity. *Neuron* 54: 291–301.
59. Van Ooyen A (2001) Competition in development of nerve connections: a review of models. *Network* 12: R1–R47.
60. Fusi S, Drew PJ, Abbott LF (2005) Cascade models of synaptically stored memories. *Neuron* 45: 599–611.
61. Busetto G, Higley MJ, Sabatini BL (2008) Developmental presence and disappearance of postsynaptically silent synapses on dendritic spines of rat layer 2/3 pyramidal neurons. *J Physiol (Lond)* 586: 1519–1527.
62. Zito K, Scheuss V, Knott G, Hill T, Svoboda K (2009) Rapid functional maturation of nascent dendritic spines. *Neuron* 61: 247–258.
63. Nägerl UV, Köstinger G, Anderson JC, Martin KAC, Bonhoeffer T (2007) Protracted synaptogenesis after activity-dependent spinogenesis in hippocampal neurons. *J Neurosci* 27: 8149–8156.
64. Gasparini S, Saviane C, Voronin LL, Cherubini E (2000) Silent synapses in the developing hippocampus: Lack of functional ampa receptors or low probability of glutamate release? *Proc Natl Acad Sci U S A* 97: 9741–9746.
65. Hanse E, Gustafsson B (2001) Quantal variability at glutamatergic synapses in area cal of the rat neonatal hippocampus. *J Physiol (Lond)* 531: 467–480.
66. Cohen-Cory S (2002) The developing synapse: Construction and modulation of synaptic structures and circuits. *Science* 298: 770–776.
67. Bourjaily MA, Miller P (2011) Excitatory, inhibitory, and structural plasticity produce correlated connectivity in random networks trained to solve paired-stimulus tasks. *Front Comput Neurosci* 5: 37.
68. Keck T, Mrsic-Flogel TD, Vaz Afonso M, Eysel UT, Bonhoeffer T, et al. (2008) Massive restructuring of neuronal circuits during functional reorganization of adult visual cortex. *Nat Neurosci* 11: 1162–1167.